Investigation of water-retention and uniaxial compression behaviour of MX80 bentonite pellet at various suctions

Jin-Wen Yang[1*], *Yu-Jun* CUI[1], *Nadia* Mokni[2]

[1]Ecole des Ponts ParisTech, Laboratoire Navier/CERMES, 6 et 8 avenue Blaise Pascal, 77455 Marne La Vallée cedex 2, France
[2]Institut de Radioprotection et de Sûreté Nucléaire (IRSN), PSE-ENV/SEDRE/LETIS, Fontenay-aux-Roses, 92260, France

Abstract. MX80 bentonite pellet/powder mixture has been regarded as a candidate sealing material in deep geological high-level radioactive waste disposal. As single pellet plays an important role in the global hydro-mechanical behaviour of the mixture, a series of single pellet compression tests were conducted on cylinder-shape MX80 bentonite 32-mm pellet after reaching suction equilibrium. The changes in volume and water content during the suction equilibration with the vapour equilibrium technique allowed the water-retention properties to be investigated. X-ray μCT observations were also made on pellets after reaching the target suctions. Results showed that upon drying the water content, void ratio and volumetric strain decreased slightly, but increased significantly upon wetting. Moreover, upon drying the network of cracks presented insignificant change and the cracks were mainly located in the marginal areas of pellet, while on wetting, cracks substantially propagated from the marginal areas to the core of pellet. The uniaxial compression tests on single pellets showed that the axial strain ε_{axial} contributed to the contractancy, while the lateral strain $\varepsilon_{lateral}$ to the dilatancy. The uniaxial shear strength $\sigma_{a,\,max,}$ the crack closure (CC) stress σ_{cc}, the crack initiation (CI) stress $\sigma_{ci,}$ the crack damage (CD) stress σ_{cd} and the Young's modulus E were found to decrease with suction decreasing, evidencing the suction effect through softening and cracking. Because of the combined effect of suction and wetting-induced cracks, the Poisson's ratios v increased until the suction decreased to 38-25 MPa, and then decreased with further suction decrease. Uniaxial loading closed the horizontal wetting-induced cracks at suctions ≤ 9 MPa, leading to a drop of $\varepsilon_{lateral}$ before CC.

1 Introduction

Bentonite pellet/powder mixture has been regarded as a promising option to build buffers, backfills and seals in geological disposal facilities of high-level and intermediate-level radioactive wastes thanks to its high swelling capacity, low permeability, high radionuclide retention capacity and easy manufacture and installation [1–3]. SEALEX (SEALing Experiment) and VSEAL (Vertical SEALing) projects launched by the French Institute for Radiation Protection and Nuclear Safety (IRSN), aim to investigate the long-term performance of swelling clay-based sealing systems in the context of geological high-level radioactive waste disposal. In the SEALEX and VSEAL projects, MX80 bentonite pellet/powder mixture, made up of large-sized (32 mm or 7 mm) bentonite pellets and small-sized (< 2 mm) bentonite powder (80/20 in dry mass), has been considered [4, 5]. As bentonite pellets play an important role in the behaviour of pellet/powder mixture, it appears essential to well understand the behaviour of individual pellets.

Microstrucutre and water-retention behaviour of 7-mm MX80 bentonite pellets were investigated by a series of tests including micro-computed tomography (μCT), mercury intrusion porosimetry (MIP) and water retention [4, 6, 7]. It was observed that upon wetting, water content increased linearly with suction decrease, together with pellet swelling and wetting-induced cracks. They attributed the pellet swelling to the combined effects of macro-scale crack propagation and nano-scale bentonite grains swelling. Darde et al. [8] performed uniaxial compression tests on single original MX80 bentonite 7-mm with a central cylinder-shaped part and two spherical caps on the top and bottom, at suctions ranging from 82 to 9 MPa in the axial and radial directions, which were the point-to-point and line-to-line contacts, respectively. Young's modulus was estimated by assuming isotropic linear elastic behaviour and taking a Poisson' ratio equal to 0.3. They found that significant decreases of Young's modulus and shear strength were induced by wetting. The uniaxial compressions were furthered on single original MX80 bentonite 32-mm pellets equilibrated under suctions from 113 to 4.2 MPa, in the point-to-point contact [9]. Photographs revealed that pellets under compression were broken along a penetrative crack stretching from the top contact point to the bottom one after reaching the peak axial stress, regardless of the imposed suctions. Given the difficult-to-determine stress state in the point-to-point contact, the normal contact stiffness that was defined as the ratio of force to displacement instead of Young's modulus and Poisson's ratio was studied [9]. Therefore, the Young's modulus and Poisson's ratio

*Corresponding author: jinwen.yang@enpc.fr

cannot be determined directly and the cracking behaviour of MX80 bentonite pellet during compression was difficult to track because the point-to-point and line-to-line contacts led to a stress state difficult to determine.

In this study, the top and bottom caps of original 32-mm MX80 bentonite pellets were removed to make them become cylinder-shaped to well define the stress state. These pellets were equilibrated at various suctions under free swelling condition, with the changes in volume and water content recorded. Then, a series of uniaxial compression tests were performed on these cylinder-shaped pellets by the face-to-face contact, with measurements of axial force, axial and lateral displacements. Based on the test results, the water-retention and uniaxial compression behaviours were clarified. Moreover, crack closure, crack initiation and crack damage were determined to help clarify the elastic properties and the cracking behaviour during compression. The effects of suction and wetting-induced cracks were also analyzed.

2 Materials and methods

2.1 Materials

MX80 bentonite was considered, which was taken from Wyoming, USA. This bentonite contains smectite (80%) and some other non-clayey minerals, including 8% anorthite, 4% quartz, 4% muscovite, 2% albite and < 1% pyrite [4]. Several sizes of MX80 bentonite pellet are manufactured by the Laviosa-MPC company and the pellet adopted here is approximately 32 mm in diameter. In the fabrication process, bentonite powder was forcefully and rapidly compacted to form high-density pellets with a central cylinder-shaped part and two spherical caps on the top and bottom [4, 8]. In this study, the tested pellet is cylinder-shaped with smooth and flat surfaces. The objective of using cylinder-shaped pellets is to well determine the mechanical behaviour of pellets with a better-defined stress state. Fig. 1 presents an original and a tested pellet. The top and bottom spherical caps were firstly excised from these original pellets with a cutting machine, and then further smoothened by sandpapers. The initial suction (s = 114.36 MPa) was measured by a chilled mirror dew point tensiometer (Decagon WP4C), corresponding to an initial water content w = 6.32%. The initial diameters and heights of tens of machined pellets were measured and their average values were adopted. The initial hydro-mechanical properties of pellets are summarized in Table 1.

2.2 Experimental methods

The vapor equilibrium technique was adopted for the suction-control during the first hydration stage [10]. The cylinder-shaped pellets were carefully placed in glass pots with desired saturated salt solutions [10] inside at constant 20°C temperature, equilibrated under suctions

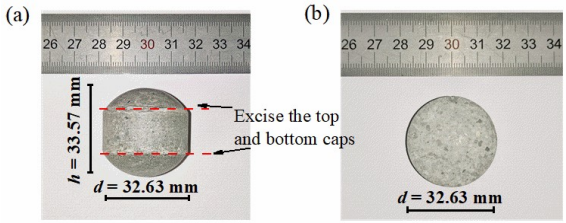

Fig. 1. MX80 bentonite pellet: (a) original pellet; (b) machined pellet.

Table 1. Initial hydro-mechanical properties of pellets

Property	Value
Dry density, ρ_d: Mg/m^3	2.08
Void ratio, e	0.368
Water content, w %	6.32
Diameter, D: mm	32.66
Height, H: mm	11.81
Suction, s: MPa	114.36

from 262 to 4.2 MPa. The mass, height and diameter of each pellet were measured regularly for the calculation of void ratio, volumetric strain and water content to assess whether the pellet reaches the target suction. After pellets reaching their target suctions, one pellet under each suction was waxed to avoid water loss by evaporation for future μCT scans by Skyscanner-1173. The voltage and current of X-ray sources are 130 kV and 61 μA respectively, with a 0.25mm-thick copper filter placed in front of the sources. The whole pellet was scanned using 2240 × 2240 pixels into 16-bit BMP-format images with voxel size = 18 μm. After scans, the bentonite pellet was 3D reconstructed by assembling around 700 horizontal slices with Bruker software NRecon with median noise reduction. Three other pellets under each suction were taken out for the uniaxial compression tests. One force transducer of 25 kN under the bottom platen was employed to record the axial force. One linear variable differential transducer (LVDT) installed in front of the pellet with 0.1 μm resolution was used to record the vertical displacement and two others on both sides of the pellet for the lateral displacement. The pellet was firstly placed between two parallel platens, and then compressed at a constant rate of 0.1 mm/min at constant 20°C temperature [8]. After the compression tests, the logged data in terms of axial force and axial and lateral displacements were extracted for further analysis.

3 Results and discussion

3.1 Water retention behaviour

The variation of water content versus elapsed time is shown in Fig. 2(a). The lockdown of France in March and April 2020 led to the absence of data from the 30th to 100th day, except for the pellets at target suctions 113 and 57 MPa that were prepared after the lockdown. It is observed that all pellets reached suction equilibrium after three months except the pellets at target suctions 113 and 57 MPa with less than one month. Fig. 2(b)

shows the linear relationship between water content and suction after reaching suction equilibrium - water content increased linearly with suction decrease.

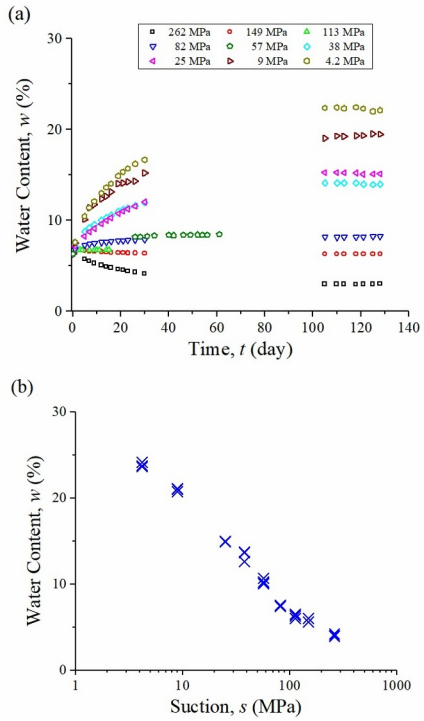

Fig. 2. (a) Variations of water content during suction equilibrium; (b) Water content versus suction.

Fig. 3 shows the μCT images of horizontal and vertical slices of the middle positions of bentonite pellets equilibrated under various suctions. It appears that the morphology of pellets at suctions ≥ 82 MPa was almost the same with limited cracks and without significant shrinkage. A slight swelling and plenty of wetting-induced cracks started to occur at suction 57 MPa. The swelling and cracking further developed upon further wetting, in agreement with the μCT observation of [7] on MX80 bentonite 7-mm pellets. As the pellets were wetted at suctions ≤ 9 MPa, a larger swelling was identified and the wetting-induced cracks became more and more significant, with a few large cracks of lengths of several millimeters. The horizontal cracks on the vertical slices were identified for all suctions from 262 to 4.2 MPa (Fig. 3). The lower the suction, the larger and the much more the horizontal cracks.

The axial strain ε_{axial} and lateral strain $\varepsilon_{lateral}$ were determined by dividing the height and diameter by the initial values, respectively. The volumetric strain ε_v was calculated as follows:

$$\varepsilon_v = \varepsilon_{axial} + 2 \times \varepsilon_{lateral} \quad (1)$$

The relationship between strains and suction after suction equilibrium is shown in Fig. 4, confirming that the change in size was small at high suctions ≥ 82 MPa, while such change gradually increased with the suction decrease from 57 to 4.2 MPa.

3.2 Uniaxial compression behaviour

The compression-induced ε_{axial} and $\varepsilon_{lateral}$ were calculated by dividing the current variations of height and diameter by the corresponding values right before the compression test. The axial stress σ_a was calculated by the force divided by the real-time contact area between

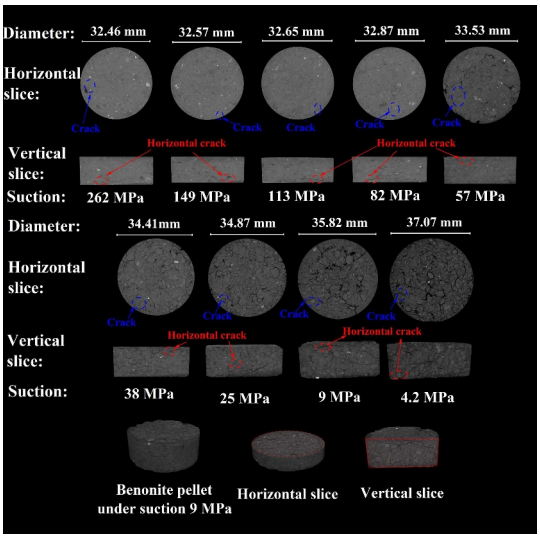

Fig. 3. μCT images of bentonite pellets equilibrated under various suctions: (a) 262-82 MPa; (b) 57-4.2 MPa.

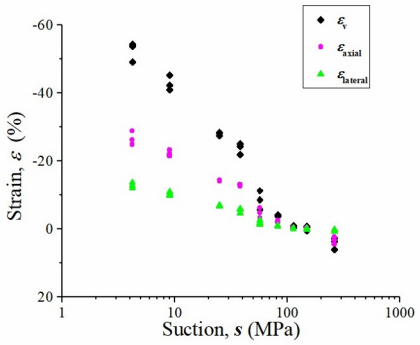

Fig. 4. Axial, lateral and volumetric strains versus suction.

the bentonite pellet and the top platen. As mentioned previously, three parallel tests were conducted for each suction. Fig. 5 illustrates the mechanical responses of the pellets at different suctions. From Fig. 5(a), obvious peaks can be identified on the σ_a-ε_{axial} curves when suction was higher than 25 MPa, and the higher the suction the more pronounced the peak. Fig. 5(b) shows that a general behavior of contractancy followed by dilatancy was observed for all suctions. The suction effect appeared slight on the contractancy, but strong on the dilatancy - the higher the suction the larger the dilatancy, consistent with the results of [11]. Moreover, the initial slopes of ε_v-ε_{axial} curves were almost 1:1, suggesting that initial contractancy behaviour mainly came from the axial strain ε_{axial}, the lateral strain $\varepsilon_{lateral}$ approaching zero. The $\varepsilon_{lateral}$ contributed to the dilatancy mainly. It appears from Fig. 5(c) that suction had a positive effect on the $\varepsilon_{lateral}$ - the higher the suction the larger the $\varepsilon_{lateral}$. In addition, the sudden drop of $\varepsilon_{lateral}$ at the initial stage was observed only at suctions 9 and

4.2 MPa and the continuous decrease of $\varepsilon_{lateral}$ at suction 4.2 MPa.

The maximum axial stress $\sigma_{a,\,max}$ is named as the uniaxial shear strength because of the lateral stress equal to zero in this study. Fig. 6 shows the change in uniaxial shear strength $\sigma_{a,\,max}$ with suction in a log-log plot. There was no significant change when the suction decreased from 262 to 113 MPa. However, the $\sigma_{a,\,max}$ remarkably decreased from 82 to 9 MPa. The change of $\sigma_{a,\,max}$ became slight again when suction was lower than 4.2 MPa. A fitting curve can be plotted with suctions 82 and 9 MPa as two turning points. Thereby, three zones can be defined: a high-suction zone with suctions ≥ 82 MPa, a low-suction zone with suctions ≤ 9 MPa, and a transition zone with suctions in between.

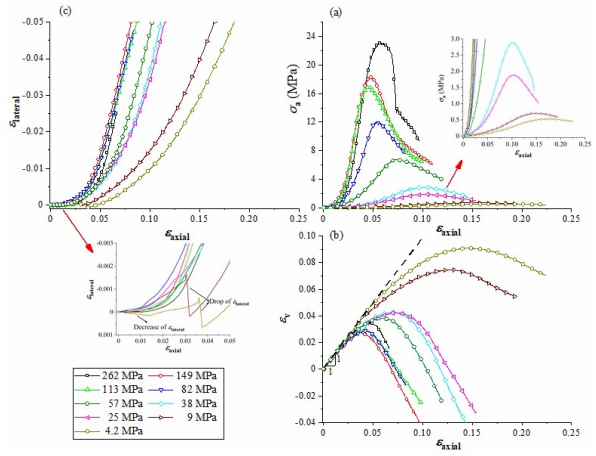

Fig. 5. Compression test results for different suctions.

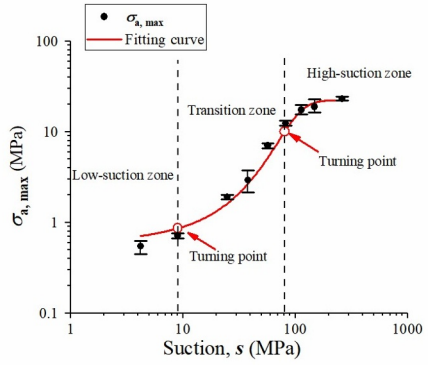

Fig. 6. Uniaxial shear strength $\sigma_{a,\,max}$ versus suction.

3.3 Determination of crack closure and crack initiation

Plenty of studies on the cracking behaviour of rocks or soils by unconfined compression tests were reported [12–14]. Five stages were defined on the stress-strain curve with four characteristic crack stresses - Crack closure (CC) stress σ_{cc}, Crack initiation (CI) stress σ_{ci}, Crack damage (CD) stress σ_{cd} and $\sigma_{a,\,max}$, as depicted in Fig. 7 (pellet at suction 113 MPa taken as an example): Stage I: crack closure stage, Stage II: elastic stage, Stage III: stable crack growth stage, Stage IV: unstable cracking stage and Stage V: post-peak stage. The CC was the end of the pre-existing cracks closing process and the beginning of elastic deformation. The CI represented the stress level where micro-fracturing begins and was considered as the point where the lateral and volumetric strain curves depart from linearity. Crack propagation can be considered as being either stable or unstable. The unstable conditions suggested that crack growth emerged from the point of reversal on the ε_v-ε_{axial} curves and such point was known as the CD. The stable crack growth stage began from σ_{ci} and ended at σ_{cd}.

The Continuous Strain Deviation (CSD) method proposed by [15] was applied on the σ_a-$\varepsilon_{lateral}$ curves, with a point on the σ_a-$\varepsilon_{lateral}$ curve which corresponds to approximately 40% of the maximum axial stress $\sigma_{a,\,max}$. The σ_{cc} and σ_{ci} under different suctions were then determined with σ_{cd} and $\sigma_{a,\,max}$ also shown in Fig. 8. Thereby, five stages (crack closure stage, elastic stage, stable crack growth stage, unstable cracking stage and post-peak stage) can be visualized in this figure for different suctions.

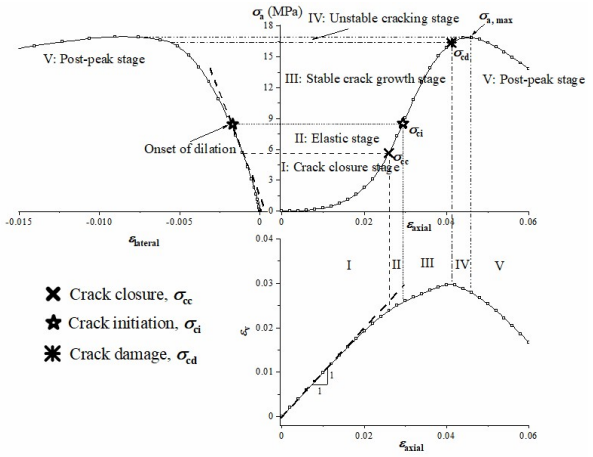

Fig. 7. Stage division on stress-strain curve and onset of dilatancy, for 113 MPa suction.

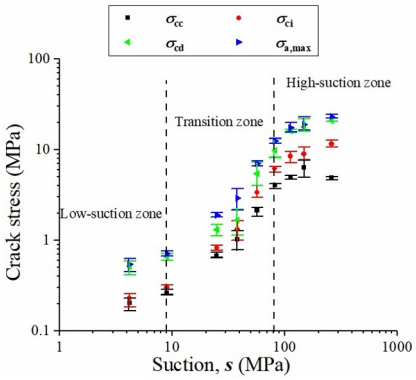

Fig. 8. Characteristic crack stresses versus suction.

3.4 Elastic behaviour

The elastic parameters including Young's modulus E and Poisson's ratio v, were calculated within the elastic stage (Stage II) by Eq. (2) and Eq. (3):

$$E = \frac{\Delta\sigma_a}{\Delta\varepsilon_{axial}} \quad (2)$$

$$v = -\frac{\Delta\varepsilon_{lateral}}{\Delta\varepsilon_{axial}} \quad (3)$$

The variations of E and ν with suction are depicted in Fig. 9. It appears that E and $\sigma_{a,\,max}$ varied with suction following the similar trend, in agreement with the observation of [14]. In general, E and $\sigma_{a,\,max}$ decreased significantly with the suction decrease because of the increasing wetting-induced cracks and deformability. The variation of Poisson's ratio ν was quite different: ν increased as suction decreased from 262 to 38 MPa, but it decreased from 25 to 4.2 MPa suction. ν of the Opalinus Clay decreased upon suction increasing [14]. Kumar [16] found that ν would increase with the decrease in the volume of cracks. This showed that the variation of ν was dependent on suction and cracks. As $\Delta\varepsilon_{axial}$ was fixed due to the constant loading rate of the test apparatus platen, $\nu = \Delta\varepsilon_{lateral}$. Thus, the variation of ν resulted from the competition of suction and wetting-induced cracks through affecting $\Delta\varepsilon_{lateral}$. As the suction effect predominated with the suction decrease from 262 to 38 MPa, the pellets became softer, leading to a larger magnitude of $\Delta\varepsilon_{lateral}$ ($\varepsilon_{lateral}$ and $\Delta\varepsilon_{lateral}$ are negative values), bringing in ν increasing, while the effect of wetting-induced cracks prevailed as the suction decreased from 25 to 4.2 MPa, large wetting-induced cracks undermined the magnitude of $\Delta\varepsilon_{lateral}$, leading to ν decreasing.

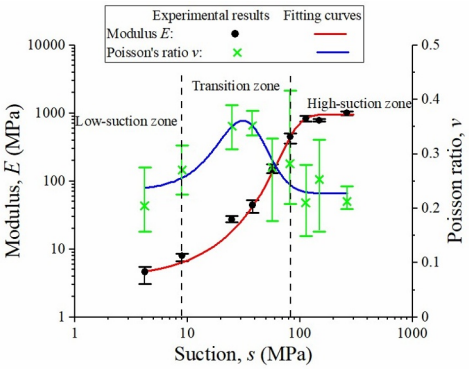

Fig. 9. Young's modulus E and Poisson's ratio ν versus suction.

3.5 Cracking behaviour

Pre-existing cracks occurred due to the fabrication and suction-control wetting, giving rise to a strong non-linearity in the crack closure stage (Stage I). These cracks affected $\sigma_{a,\,max}$, E, ν, ε_{axial}, $\varepsilon_{lateral}$ and ε_v. The $\sigma_{a,\,max}$ marked the onset of post-peak behaviour from which failure forms; the sudden drop of σ_a after its peak (Fig. 7) was due to the macro-crack or failure propagation. The wetting-induced horizontal cracks in the vertical slices (Fig. 3) that are vertical to the compressive loading direction, were observed at all suctions. The lower the suction, the larger and the much more the wetting-induced horizontal cracks. The crack closure stage (Stage I) corresponds to the closure of the wetting-induced horizontal cracks under the compressive loading. Specifically, the drops of $\varepsilon_{lateral}$ at suctions 9 and 4.2 MPa in the crack closure stage resulted from the closure of large wetting-induced cracks (Fig. 5(c)). The decrease of $\varepsilon_{lateral}$ at suction 4.2 MPa was due to the closure of some relatively smaller wetting-induced horizontal cracks. However, at higher suctions ≥ 25 MPa, both the number and sizes of cracks were too small to generate a decrease or a drop of $\varepsilon_{lateral}$ before the CC. Note that the sudden drop or decrease of $\varepsilon_{lateral}$ in Fig. 5(c) can also confirm the observation of [17] - $\varepsilon_{lateral}$ was more sensitive than ε_{axial} to the growth of cracks. The general trends of stress-strain curves were similar to those of other literatures [12, 17–19]. However, the initial slopes of σ_a-ε_{axial} and $\varepsilon_{lateral}$-ε_{axial} curves (Figs. 5(a) and 5(c)) were much smaller than those of other literatures due to the larger axial strain and smaller lateral strain initially which resulted from the crack closure in Stage I and the large ends' friction, respectively.

Fig. 8 shows the positive correlation between three characteristic crack stresses (σ_{cc}, σ_{ci} and σ_{cd}) and suction, in agreement with the results obtained by [14] on Opalinus Clay. Moreover, suction decreasing narrowed the difference between σ_{cc} and σ_{ci}. Three zones can be clearly identified with suctions 82 and 9 MPa as two turning points. Fig. 10 presents the stress ratios of σ_{cc}, σ_{ci} and σ_{cd} to $\sigma_{a,\,max}$, which were employed to describe the positions of the CC, CI and CD relative to the maximum axial stress $\sigma_{a,\,max}$. It appears that the CC was slower to come upon suction decreasing, as opposed to the CI, showing that the elastic stage (Stage II) became smaller and stable tensile cracks were earlier to occur upon wetting. With more wetting-induced cracks, a longer stage was needed to close the cracks and a shorter time was required for stable tensile cracks to occur. Comparison between Figs. 9 and 10 shows that the variation of CD with suction presented an opposite trend with respect to that of Poisson' ratio ν. This indicated that the larger ν value brought in the CD earlier to occur. The CI was caused by stable tensile cracks, while the CD was caused by unstable shear cracks [12, 13, 19, 20]. It showed that the larger the ν value, the larger the $\Delta\varepsilon_{lateral}$ value, the earlier the unstable shear cracks to come.

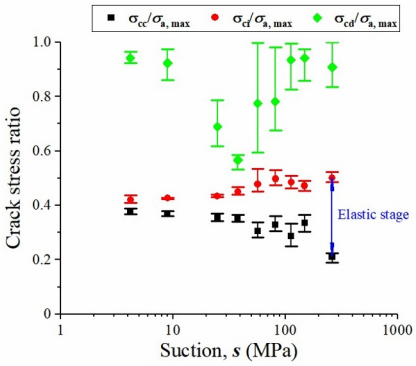

Fig. 10. Characteristic crack stress ratios versus suction.

4 Conclusions

Original MX80 bentonite pellets were machined to cylindrical shape in order to simplify the measurement of axial stress in uniaxial compression tests. After machining, the pellets were equilibrated under different suctions. The results of water-retention and uniaxial compression behaviours were then analysed.

Upon wetting, water content increased linearly with suction decrease, with cracks generated. The

morphology of pellets at suctions ≥ 82 MPa was almost the same with limited cracks, without significant shrinkage. Swelling and wetting-induced cracking started at suction 57 MPa and further developed upon further suction decrease. In particular, a few cracks as long as several millimeters were observed at suctions ≤ 9 MPa.

For all suctions, a general behavior of contractancy followed by dilatancy was observed. The suction effect appeared slight on the contractancy, but strong on the dilatancy. Initial contractancy mainly came from axial deformation, while lateral deformation mainly contributed to dilatancy.

The $\sigma_{a,\,max}$, σ_{cc}, $\sigma_{ci,}$ $\sigma_{cd,}$ E and the range of elastic stage (Stage II) delimited by CC and CI all decreased with suction decreasing, due to the wetting-induced cracking and stiffness decreasing. They showed no significant change in the high-suction zone between 262 and 82 MPa and the low-suction zone between 9 and 4.2 MPa, but decreased remarkably in the transition zone from 82 to 9 MPa. 82 and 9 MPa suctions are two turning points.

The closure of large wetting-induced horizontal cracks at suction 9 or 4.2 MPa led to a drop or decrease of $\varepsilon_{lateral}$ in the crack closure stage (Stage I). Both suction and wetting-induced cracks affected the Poisson's ratio v through $\Delta\varepsilon_{lateral}$. The larger the v value, the earlier the occurring of the CD.

References

1. R. Pusch, Nucl Technol **45**, 153–157 (1979)
2. E. E. Alonso, E. Romero, C. Hoffmann, E. García-Escudero, Eng. Geol. **81**, 213–226 (2005)
3. Y. J. Cui, J. Rock Mech. Geotech. Eng. **9**, 565–574 (2017)
4. A. Molinero Guerra, N. Mokni, P. Delage, Y. J. Cui, A. M. Tang, P. Aimedieu, F. Bernier, M. Bornert, Appl. Clay Sci. **135**, 538–546 (2017)
5. A. M. Alcantara, N. Mokni, E. Romero, S. Olivella, E3S Web Conf. **195**, (2020)
6. A. Molinero Guerra, Y. J. Cui, Y. He, P. Delage, N. Mokni, A. M. Tang, P. Aimedieu, M. Bornert, F. Bernier, Eng. Geol. **248**, 14–21 (2019)
7. A. Molinero-Guerra, P. Delage, Y. J. Cui, N. Mokni, A. M. Tang, P. Aimedieu, F. Bernier, M. Bornert, Geotechnique **70**, 199–209 (2020)
8. B. Darde, A. M. Tang, J. M. Pereira, J. N. Roux, P. Dangla, J. Talandier, M. N. Vu, Geotech. Lett. **8**, 330–335 (2018)
9. Z. Zhang, Y. J. Cui, J. Yang, N. Mokni, W. M. Ye, Y. He, Acta Geotech. **17**, 2435–2447 (2021)
10. A. M. Tang, Y. J. Cui, Can. Geotech. J. **42**, 287–296 (2005)
11. Y. J. Cui, P. Delage, Geotechnique **46**, 291–311 (1996)
12. C. D. Martin, N. A. Chandler, Int. J. Rock Mech. Min. Sci. **31**, 643–659 (1994)
13. M. Nicksiar, C. D. Martin, Rock Mech. Rock Eng. **47**, 1165–1181 (2014)
14. K. M. Wild, L. P. Wymann, S. Zimmer, R. Thoeny, F. Amann, Rock Mech. Rock Eng. **48**, 427–439 (2015)
15. D. Wang, S. He, D. D. Tannant, KSCE J. Civ. Eng. **23**, 1819–1828 (2019)
16. J. Kumar, Proc. - SPE Annu. Tech. Conf. Exhib. **1976-Octob**, (1976)
17. M. Nicksiar, C. D. Martin, Rock Mech. Rock Eng. **45**, 607–617 (2012)
18. M. Cai, P. K. Kaiser, Y. Tasaka, T. Maejima, H. Morioka, M. Minami, Int. J. Rock Mech. Min. Sci. **41**, 833–847 (2004)
19. F. Amann, E. A. Button, K. F. Evans, V. S. Gischig, M. Blümel, Rock Mech. Rock Eng. **44**, 415–430 (2011)
20. E. Eberhardt, D. Stead, B. Stimpson, R. S. Read, Can. Geotech. J. **35**, 222–233 (1998)